Spectral Characterization of Modern Spacecraft Materials

Heather M. Cowardin[1]
Jacqueline A. Reyes[2], Elena A. Plis[3,5], Ryan C. Hoffmann[4], Gregory P. Badura[3], Jainisha R. Shah[5], Sydney E. J. Collman[5], Miles T. Bengtson[6], Daniel P. Engelhart[7], Timothy R. Scott[8]

[1] NASA Johnson Space Center, Orbital Debris Program Office, Houston, TX, 77058, USA, Heather.Cowardin@nasa.gov
[2] University of Texas at El Paso, TX, 79968, USA
[3]Georgia Tech Research Institute (GTRI), Atlanta, GA, 30318, USA
[4]Air Force Research Laboratory, Space Vehicles Directorate, Kirtland AFB, Albuquerque, NM, 87117, USA
[5]Assurance Technology Corporation, Carlisle, MA, 01741, USA
[6]National Research Council Research Associateship Program, Kirtland AFB, NM, 87117, USA
[7]University of New Mexico, Albuquerque, NM, 87106, USA
[8]DuPont de Nemours, Inc., Durham, NC, 27703, USA

ABSTRACT

One of the observational parameters of interest in ground-based optical measurements is ascertaining material properties using broadband filter photometry and spectroscopy for orbiting targets. Broadband photometry can provide reflectance measurements that can aid in producing color-color indices and assess if objects can be classified into families or taxonomies. However, these reflectance properties can vary due to aspect angle, phase angle, and general degradation of the target's exterior material. Spectral characterization can aid in material characterization utilizing known absorption bands and spectral signatures, but these signatures are affected by the same conditions described for remote observations. When utilizing ground-based measurements, it is well understood that material characterization is subject to variability due to space weathering and/or other external events (i.e., collision or explosion). The focus of this study is on space weathering effects on spacecraft materials in low Earth orbit.

To better assess how materials are affected by the harsh space environment, specifically modern materials, a collection of materials were analyzed in both their pristine condition and after electron bombardment. This sample collection is part of an upcoming mission with the Materials International Space Station Experiment Flight Facility (MISSE-FF) that will be launched in 2022. These laboratory analyses on the samples will provide a ground-truth to compare with the *in situ* collected data. The data will also be stored in the NASA Johnson Space Center's Spacecraft Materials Spectral Database that is available to U.S. citizens and maintained by the Orbital Debris Program Office.

The following paper provides an overview of the materials investigated, laboratory, and database overview, and spectral results for both pristine and post-electron exposed conditions. The spectral signature data highlights which materials are stable, or remain relatively unchanged, and which materials vary significantly due to exposure and material configuration (variations due to rotation of the sample on a flat surface). Initial results on changes in spectral directional reflectance of the materials as a function of incident illumination direction are also presented. This data also will benefit the space situational awareness community with spectral characterization of novel materials that can support their respective optical measurements focused on material identification.

1. INTRODUCTION

Characterization of spacecraft materials has been an important focus for the broad Space Situational Awareness/Space Domain Awareness (SSA/SDA) community since the dawn of flight. Understanding the durability, survivability, degradation, and variations in material properties is key to supporting space flight, mitigating the growth of orbital debris, and supporting material identification from an environmental awareness standpoint. The NASA Orbital Debris

Program Office (ODPO) has utilized radar, optical, and *in situ* measurements to assess the orbital environment and provide updated engineering models to the community. With the evolving technology used in spacecraft design and the increased availability of modern materials, it is critical to analyze these new materials to determine the effectiveness in a harsh space environment, specifically materials exposed to electron bombardment, ultraviolet (UV) radiation, and atomic oxygen (AO).

Since 2001, the International Space Station (ISS) has opened opportunities to host payloads on the external surface to study the harsh space environment in low Earth orbit (LEO). One of these flight experiments, Materials International Space Station Experiment (MISSE) - Flight Facility (MISSE-FF) has flown 4,000 materials in various MISSE missions [1, 2]. In May 2020, a collaborative effort with members from the Georgia Tech Research Institute (GTRI), the Air Force Research Laboratory (AFRL), the NASA ODPO, the University of Texas - at El Paso, and DuPont de Nemours, Inc., was initiated via a proposal entitled "Spectral Characterization of Novel Spacecraft Materials at LEO Environment" to host selected materials on an upcoming MISSE-FF opportunity. In June 2020, a letter of acceptance for this mission was provided and the team has been working diligently to conduct ground-test on a subset of novel materials which will be hosted on the upcoming MISSE-FF mission slated for launch on Space X CRS-25 (July 2022). The materials will be exposed for six months, with real-time science data and photos expected daily within the first month post-installation, weekly for the next two months, and monthly for the remaining duration of the mission.

The following paper will provide an overview of the materials selected, the facilities used for the measurements/analysis, spectral characterization of the samples, and a summary of the data collected to date.

2. SAMPLES INVESTIGATED

The team evaluated various spacecraft materials, assessing classic and modern materials, best suited to provide insight into the material variations of interest to the SSA/SDA community. The team isolated the material selection to varieties of commercial polymers and polymer-hybrid materials that are promising for aerospace, avionics, and spacecraft applications, including polyimides/pyromellitic dianhydride (PMDA) sheets, carbon- and glass-fiber-reinforced (CFRP and GFRP, respectively), liquid crystal polymer (LCP) films, polyethylene terephthalate (PET) polyester films, and polyhedral oligomeric silsesquioxane (POSS) films. The polyimide (PI), LCP and PET films were all provided by DuPont, but the CFRP, GFRP, and POSS materials were purchased from spacecraft material manufacturing vendors. Fig. 1 shows a snapshot of the material integration process led by the ISS National Laboratory partner Alpha Space. The materials were mounted in exposure trays that will be exposed in the ram, zenith, and wake positions aboard the MISSE-FF. The details on the specific materials evaluated are listed in Table 1, including alumina, which is used as an optical standard for *in situ* optical measurements.

Fig. 1. Subset of MISSE-FF samples integrated into material carrier led by Alpha Space. Credit: NASA

Each of these materials were evaluated in facilities in pristine condition and after sequential electron-bombardment, AO, and UV exposure. Multiple, identical materials were used to conduct each experiment, simulating the specific conditions each material would be exposed to in space, and evaluate the resulting optical effects. For the purposes of this paper, the optical characterization will focus on materials in a pristine state and after electron-bombardment.

Table 1. Materials used for ground-based measurements and MISSE-FF mission.
Trade names and trademarks are used in this report for identification only. Their usage does not constitute an official endorsement, either expressed or implied, by the National Aeronautics and Space Administration.

ID	Name	Material Class	Density (g/cm^3)	Thickness (mils)
1	Kapton® CR	Polyimide (PI)/(PMDA)	1.54	2
2	Kapton® CS	Polyimide (PI)/(PMDA)	1.42	2
3	Kapton® WS	Polyimide (PI)/(PMDA)	1.42	1
4	Kapton® XC	Polyimide (PI)/(PMDA)	1.41	2
5	Kapton® TF	Polyimide (PI)/(PMDA)	1.42	4.0
6	200DR9	Polyimide (PI)/(PMDA)	1.42	2
7	Kapton® HN	Polyimide (PI)/(PMDA)	1.43	3
8	Economyplate™ Carbon Fiber	Carbon Fiber Reinforced Polymer (CFRP)	1.44	29
9	G-10/FR4 Glass Epoxy	Glass Fiber Reinforced Polymer (GFRP)	1.9	66
10	Zenite® LCP	Liquid Crystal Polymer (LCP)	1.75	3
11	Melinex® 454	Polyethylene terephthalate (PET)	1.4	5
12	Mylar® M021	Polyethylene terephthalate (PET)	1.39	9
13	CORIN® XLS	Polyhedral Oligomeric Silsesquioxane (POSS)	1.40	0.6
14	Thermalbright® N	Polyhedral Oligomeric Silsesquioxane (POSS)	2.08	0.8
15	Alumina	Aluminum Oxide (ALUM)	3.95	3.8

3. LABORATORY/FACILITY BACKGROUND

The pristine samples discussed in Section 2 were shipped to GTRI and NASA Johnson Space Center (JSC) to conduct optical characterization in parallel. The samples were also exposed to electron-bombardment in AFRL's environmental chamber, then those samples were sent to GTRI and NASA JSC for optical characterization. An overview of these three facilities is presented below.

3.1. Spacecraft Charging and Instrument Calibration Laboratory (AFRL-Kirtland Air Force Base)

The Spacecraft Charging and Instrument Calibration Facility (SCICL) is located at Kirtland Air Force Base in Albuquerque, New Mexico. The facility hosted the Jumbo environmental simulation chamber, a 1.8 m x 1.8 m cylindrical chamber capable of 10^{-3} torr to high vacuum of 10^{-6} torr pressures. The prime electron source is a Kimball Physics EG8105-UD electron flood gun with a range of 1 keV–100 keV. For this experiment, the MISSE-FF materials are irradiated with 100 keV electrons. Samples are mounted on a carousel allowing for multiple samples to be rotated during the high energy electrons bombardment to mitigate "hot spots" and provide equal doses, as shown in Fig. 2.

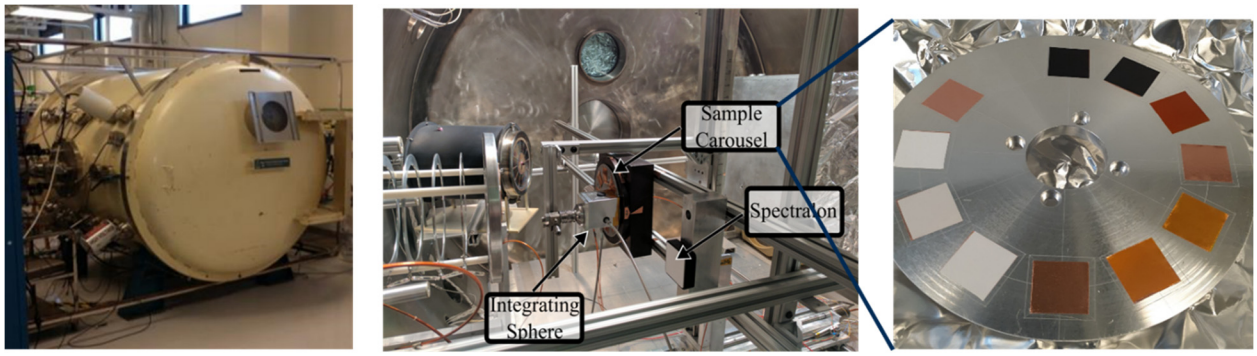

Fig. 2. SCICL Facility at AFRL-Kirtland AFB. Left image: Jumbo chamber, Center Image: Inside view of chamber, Right Image: Example of samples mounted on carousel. Credit: AFRL

3.2. Institute for Electronics and Nanotechnology/Institute for Materials (GTRI)

The Institute for Electronics and Nanotechnology/Institute for Materials is located at GTRI in Atlanta, Georgia. The facility provides instrumentation to support optical characterization and surface morphology characterization. For the former, a collection of spectrometers can be utilized, including a Thermo Nicolet™ 6700 Fourier Transform Infrared (FTIR) Spectrometer, an UV/Vis Cary 5000 Spectrometer, and an Analytical Spectral Device (ASD) FieldSpec Pro Spectrometer®, which measures radiance from 350 nm to 2500 nm and has a 20-degree solid angle. In Fig. 3, the custom optical instrumentation set-up is shown that allows Hemispherical Conical Reflectance Factor (HCRF) measurements to be acquired. This measurement allows for a laboratory approximation of true bidirectional-reflectance-distribution function (BRDF) to be acquired for selected viewing angles (0°, 30°, 60°, -30°, and -60°) and variable illumination angles from 0° to 70°.

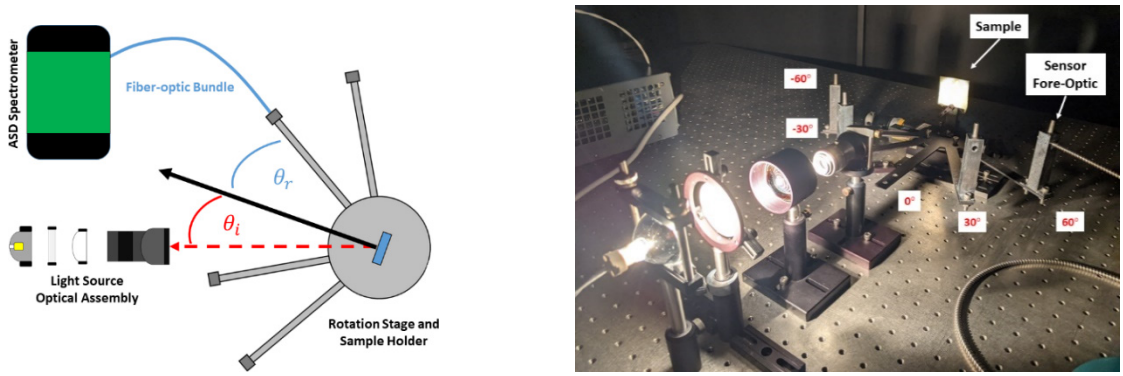

Fig. 3. The goniometer system used in this study when measuring incident irradiance and reflected radiance. (Left) A diagram of the major components showing the positioning of the spectrometer fore-optic facing the light source. (Right) An image of the setup when measuring the incident radiance onto the target plane. Credit: GTRI

3.3. Optical Measurement Center (NASA/JSC)

The Optical Measurement Center (OMC) is located at NASA JSC within the ODPO in Houston, Texas. The OMC uses an ASD FieldSpec4, providing a broad range from 350 nm to 2500 nm with ~25° field of view (FOV). A quartz lamp is used for the illumination source and a Spectralon® plate is used as the calibration source for acquiring a white reference, as shown in Fig. 4. The data are acquired in an environmentally controlled, darkroom facility and the resultant data is stored in the Orbital Debris Spacecraft Materials Spectral Database. The FieldSpec4 spectrometer can be used in field settings, provided any external light sources can be removed/powered off and a power supply is available to acquire calibrated reflectance measurements. This has proven beneficial for pre-flight spacecraft and associated materials and returned surfaces where the target of interest cannot be moved into the OMC. The OMC also can acquire broadband, photometric measurements of targets that simulate space conditions in terms of aspect angle, phase angle, and photometric filters for targets or materials of interest.

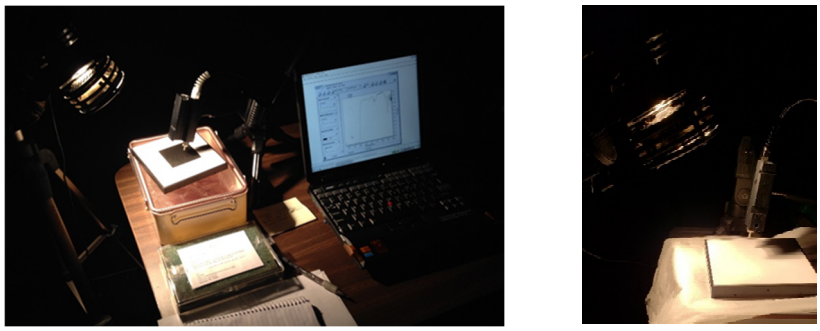

Fig. 4. Left: OMC set-up using ASD FieldSpec4, Right: Close-up image showing Spectralon for white reference calibration. Credit: NASA

4. SPECTRAL REFLECTANCE ANALYSIS

The following spectral analysis focuses on the reflectance signatures pre- and post-electron bombardment as acquired in the OMC. The samples were irradiated at AFRL in the Jumbo chamber and then stored in vacuum-sealed bags with oxygen indicators. Unfortunately, the first sample set was reported to have failed oxygen sensors, and the samples

were re-exposed, vacuum-sealed, and sent to JSC. Both series of measurements were analyzed in comparison to the pristine samples previously reported. Details of the process are provided in Table 2 courtesy of co-investigator Sydney Collman (AssurTech). Each sample was double-bagged with humectant, oxygen absorbers, and indicators, then each layer was flushed with argon to prevent oxygen exposure and mitigate aging.

Table 2. Electron exposure experimental settings from AFRL's Jumbo chamber

ID	Date	Experiment Start/Stop	FC Noise Floor	Grid set (V)	Mean Current (A)	Fluence Start (e/cm^2)	Fluence End (e/cm^2)
-	10/25/2021	7:45 AM 9:20 AM	-1.5×10^{-13}	62.5	5.4×10^{-13}	-1.4×10^{-19}	-4.75×10^{10}
A	10/26/2021	8:03 AM 12:50 pm	2.1×10^{-14}	63	1.8×10^{-13}	3.59×10^{8}	-2.018×10^{10}

In Table 3, the material identification number, name of the material, material classification, and number of rotations for each postexposure measurement ("A series" versus the initial "- series") are listed. Rotations of the material refer to rotating the sample on top of the Spectralon calibration plate approximately 90°, while taking measurements at each primary clock angle. Typically, during each measurement acquisition, the data collector rotates or moves the sample within the instrument set-up (illumination area and spectrometer fiber optic FOV) to determine if there are any spectral reflectance variations and to collect a statistically relevant number of samples (no less than three) over the entire sample. It was noted that 6 of the 15 samples did show significant differences in reflectance spectra when rotated within the illumination set-up. Note, the materials that showed significant variants are not limited to specific classes of materials. Of the six materials that were measured in rotation, three were PMDA, one was CFRP, one was PET, and one was POSS. Further characterizing these variations would be futile when laboratory-based measurements are compared to in situ data. Lastly, pristine spectral measurements of alumina were not collected in the OMC.

Table 3. List of materials analyzed in OMC after electron exposure with associated rotations

ID	Name	Material Class	Number of Rotations (A series/initial)	Visual Color Classificaiton
1	Kapton CR	Polyimide (PI)/(PMDA)	0/0	Copper/Orange
2	Kapton CS	Polyimide (PI)/(PMDA)	4/0	White
3	Kapton WS	Polyimide (PI)/(PMDA)	0/0	White
4	Kapton XC	Polyimide (PI)/(PMDA)	0/0	Black
5	Kapton TF	Polyimide (PI)/(PMDA)	5/0	Copper/Orange
6	200DR9	Polyimide (PI)/(PMDA)	0/0	Black
7	Kapton HN	Polyimide (PI)/(PMDA)	4/0	Copper/Orange
8	Carbon Fiber	Carbon fiber-reinforced Polymer (CFRP)	3/0	Black
9	Epoxy Glass	Glass fiber-reinforced Polymer (GFRP)	0/0	Blue/Green
10	Zenite LCP	Liquid Crystal Polymer (LCP)	0/0	White
11	Melinex 454	Polyethylene terephthalate (PET)	4/5	Transparent
12	Mylar M021	Polyethylene terephthalate (PET)	0/0	White
13	CORIN XLS	Polyhedral Oligomeric Silsesquioxane (POSS)	5/4	Transparent
14	Thermalbright	Polyhedral Oligomeric Silsesquioxane (POSS)	0/0	White
15	Alumina	Aluminum Oxide (ALUM)	0/0	Off-White

4.1. PMDA

Within the PI material class, the samples can be subdivided into categories based on their visual color, copper/orange, white, and black. Subdividing these samples by visible color scales will provide further clarification for absorption features noted in the polyimides that are a direct result of the surface color.

4.1.1. PMDA – Visibly Copper/Orange

The first focused area of measurements was on the PMDA Kapton sheet types: CR, TF, and HN. These materials varied in chemical compositions, but also in thickness. Kapton CR was 2 mil thick, Kapton TF was 4 mil thick, and Kapton HN was 3 mil thick, but all were close in material density (1.54 g/cm3, 1.42 g/cm3, 1.43 g/cm3), respectively. The variations are noted because thinner materials will be subject to optical interference and due to space weathering effects (or laboratory simulations), they become more difficult to characterize via reflectance spectroscopy.

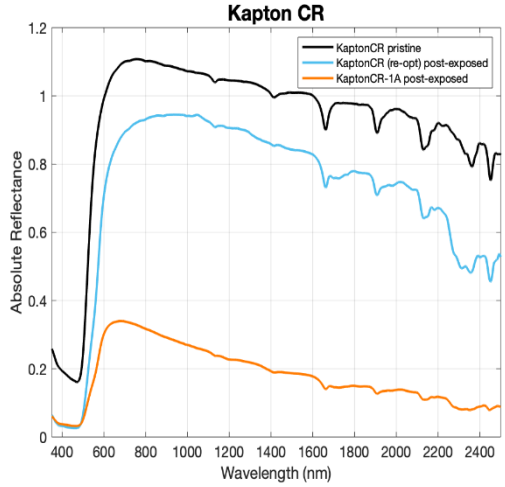

Fig. 5. Kapton CR absolute reflectance spectra data compared pre-exposure (pristine) in black versus the two post-exposure data sets in blue and orange.

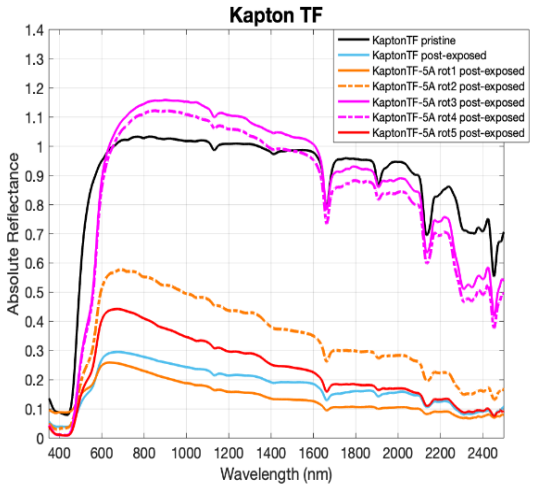

Fig. 6. Kapton TF pre-exposure (pristine) in black compared to the initial post-exposure (blue) and the A series with multiple flat rotations in the instrument set-up (orange, orange dash, magenta, magenta dash, and red).

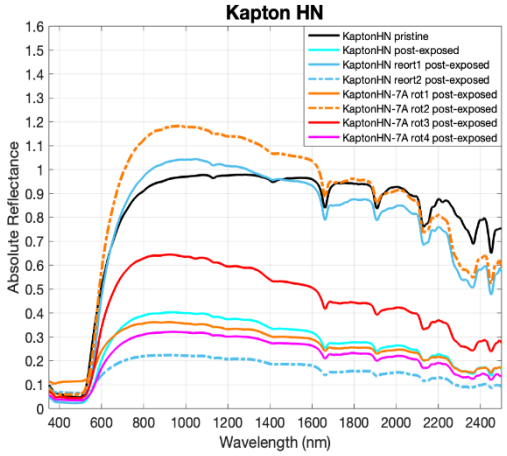

Fig. 7. Kapton HN pre-exposure (pristine) in black compared to the initial post-exposure (teal, blue, blue dash) and the A series with multiple flat rotations in the instrument set-up (orange, orange dash, magenta, and red).

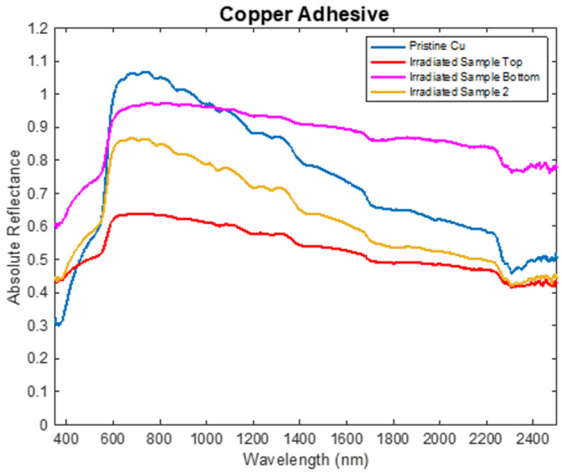

Fig. 8. Copper adhesive, pristine and after exposure. Feature between 400 nm to 600 nm is defined as the experimental bias.

All materials feature bandgap due to the amber or copper color near 450 nm to 600 nm. Typical organic features noted: O-H at 1400 nm and weak H2O at 1900 nm, C-H near 1650 nm and 2300 nm, C-H or O-H bond near 2100 nm (doublet), and 2450 nm features C-O or O-H bonds. All samples were highly reflective in their pristine state, even saturating the detector in specific orientations. Kapton CR shows a decrease in reflectivity after electron bombardment, as shown in Fig. 5 (orange curve). Kapton TF and HN post-exposed samples vary in reflectivity as the sample is

rotated within the illumination beam, illustrating both increased (specular, beyond calibration) and decreased reflectivity dependent on orientation, as presented in Figs. 6 and 7, respectively.

Of interest is the notable broad-absorption feature observed between approximately 400 nm and 550 nm. This feature is not unique to this sample or class of materials and will be discussed briefly as it is first presented in this material class. The feature is also observed in CFRP, Zenite®, Melinex®, and CORIN® spectral reflectance data. To observe a feature across multiple material classes, the experimental set-up used copper tape adhesive to mount the samples of stainless-steel pucks for the electron bombardment experiment. Materials that are optically orange/red would present a broad bandgap consistent with this regime. As shown in Fig. 8, the bandgap is associated with the copper adhesive tape and is not a spectral feature normally observed during in situ observations taken aboard MISSE. Therefore, this spectral feature will be referenced as an "experimental bias" throughout the remainder of this paper.

4.1.2. PMDA – Visibly Black

Both samples, Kapton XC and 200DR9, indicate a featureless spectral response and have a relatively low spectral response, indicative of black (light absorbing) materials as shown in Figs. 9 and 10. In addition, the thickness of these two materials are both 2 mil, therefore the spectral signatures presented are purely about material composition differences and not dependent on thickness variations. Relatively speaking, the pristine spectral response for Kapton XC ranges from approximately 20% to 50% reflectance, whereas 200DR9 is even less from 20% to 2% reflective. The pristine Kapton XC reflectance increases with higher wavelengths, whereas 200DR9 has a near exponential decrease in the visible regime. Both exposed PMDA samples show an overall decrease in reflectivity, ~55% in the visible regime, but beyond 800 nm, the delta for Kapton XC is 70% to 90%, whereas 200DR9 aligns with one of the exposed samples. The feature between 400 nm to 600 nm in the exposed 200DR9 sample is due to the experimental bias.

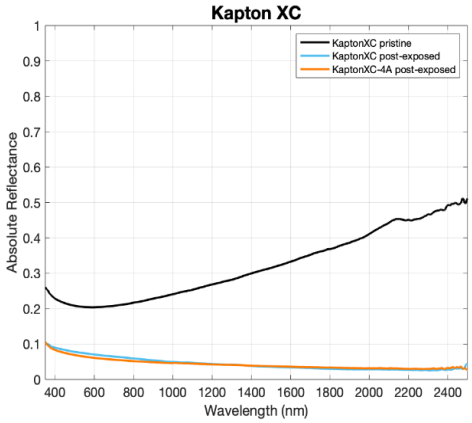

Fig. 9. Kapton XC pre-exposure (pristine) in black compared to the initial post-exposure (blue) and the A series (orange).

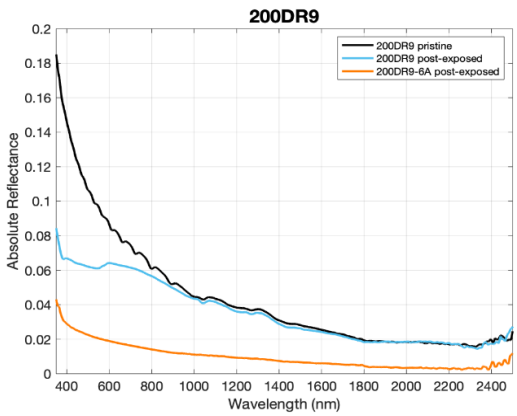

Fig. 10. 200DR9 pre-exposure (pristine) in black compared to the initial post-exposure (blue) and the A series (orange).

4.1.3. PMDA – Visibly White

The Kapton CS and Kapton WS PMDA samples are optically white, as indicated with the sharp bandpass near 350 nm to 500 nm shown in Figs. 11 and 12. The Kapton CS is 1 mil thicker than the WS, but the density of both materials is equivalent. The exposed Kapton CS varies from exceeding 100% reflectance (specular) to a decrease of 25% or 85%, making organic features harder to discern in the exposed samples as they are reoriented in the experimental set-up. For the Kapton WS exposed samples, the single absorption feature present at ~1650 nm transformed and resulted in a doublet absorption feature exhibited by the irradiated polyimide at this same wavelength. This can likely be attributed to alterations of the chemical bonds within the polymeric material, due to absorptive characteristics in the infrared regime related to organics, and after being exposed to high energy electron radiation.

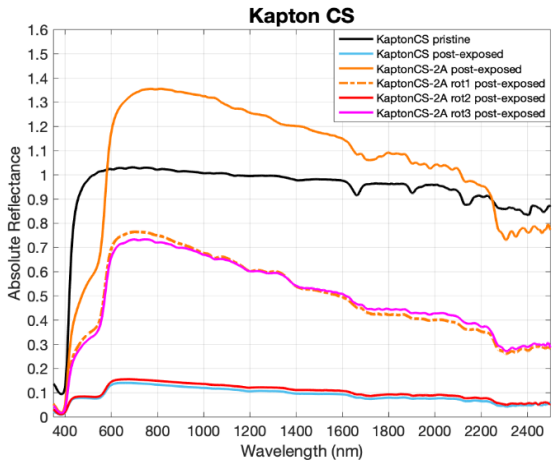

Fig. 11. Kapton CS pre-exposure (pristine) in black compared to the initial post-exposure and the A series (blue), which was rotated 4 times (orange, dotted orange, red, and magenta).

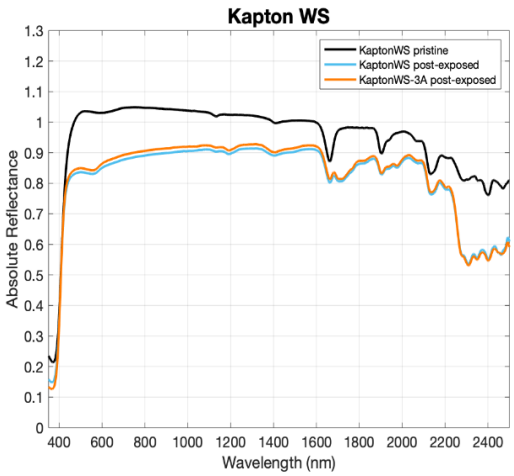

Fig. 12. Kapton WS pre-exposure (pristine) in black compared to the initial post-exposure (blue) and the A series (orange).

4.2. CFRP/GFRP

The CFRP is a modern-day spacecraft material used more commonly on spacecraft. The material is optically black and features a woven fiber pattern. Both the pristine and initial exposed material show a very close similarity in the spectral response, but the A series varies from these initial measurements for each rotation measurement collected, as shown in Fig. 13. Rotation 1 in the A-series shows the largest spectral response, with an almost 110% increase to the pristine, compared to that of rotation 3 that had only a 30% increase at 600 nm. The feature between 400 nm to 600 nm is associated with the experimental bias. In general, exposure to electron-bombardment does not significantly affect CFRP material, but the placement of the sample post-exposure did factor into overall reflectivity (increase/decrease).

The GFRP presented several organic spectral features, unlike the carbon-fiber polymer. The glass epoxy exhibits many features in the visible through near-infrared regime shown in Fig. 14. Due to the blue-green pigment used in manufacturing, the spectral reflectance peaks around 500 nm to 550 nm. There is a C-H doublet present at 1120 nm and 1200 nm, O-H or C-H at 1450 nm, C-H at 1690 nm, and O-H at 1900 nm. Electron bombardment appears to decrease the overall reflectivity across the entire spectrum.

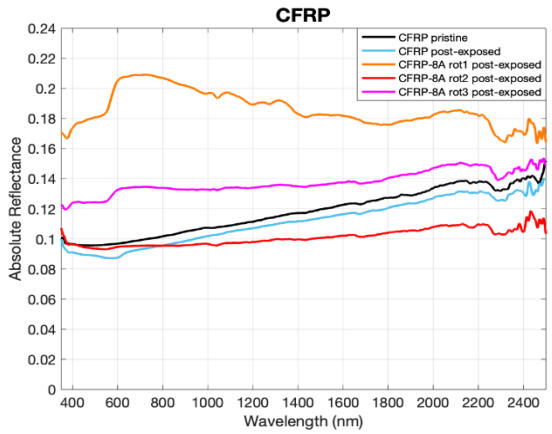

Fig. 13. CFRP pre-exposure (pristine) in black compared to the initial post-exposure (blue) and the A series with multiple flat-rotations in the instrument set-up (orange, magenta, and red).

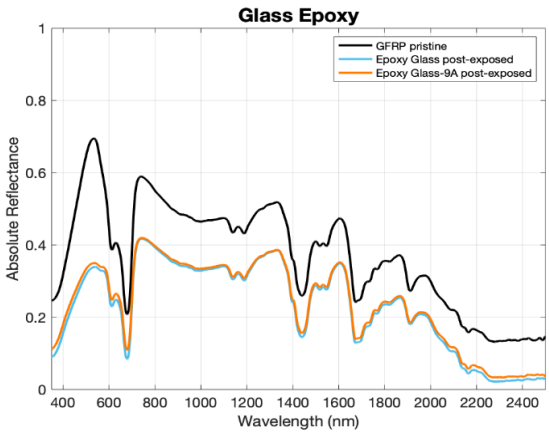

Fig. 14. Glass Epoxy pre-exposure (pristine) in black compared to the initial post-exposure (blue) and the A series (orange).

4.3. LCP

The Zenite LCP is visibly white, as evidenced by increased reflectivity at 400 nm in Fig. 15. There is an absorption feature near 1100 nm typically associated with Si. Other spectral characteristics are present that are common with organic features existing at 1400 nm, 1900 nm, 2100 nm, 2300 nm, and 2400 nm. Electron bombardment appears to decrease the overall reflectivity across the entire spectrum (similar to CFRP). The feature between 400 nm to 600 nm is due to the experimental bias mentioned previously.

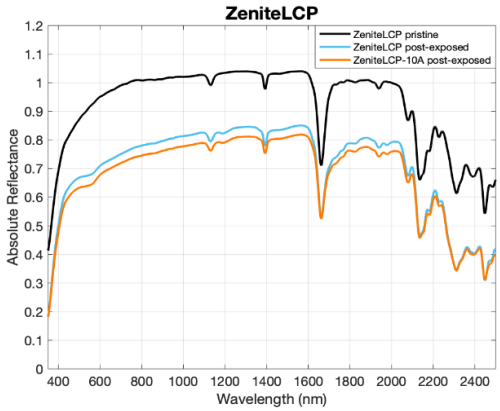

Fig. 15. Zenite LCP pre-exposure (pristine) in black compared to the initial post-exposure (blue) and the A series (orange).

4.4. PET

PET films are typically used in multi-layered insulation as passive thermal control, limiting the radiative heat transfer. Melinex 454 is a transparent film (9 mil and 10 mil) and Mylar® M021 is visibly white (3 mil and 5 mil). The Melinex 454 in its pristine state is overly featureless in the visible regime with the small bandgap noted at ~350 nm, C-H or O H bond triplet near 2100 nm, and C-H near 1650 nm and 2300 nm, as shown in Fig. 16. After the material was exposed to electron bombardment, the spectral reflectance decreased 35% to 70% in overall reflectivity. Also noted is the experimental bias.

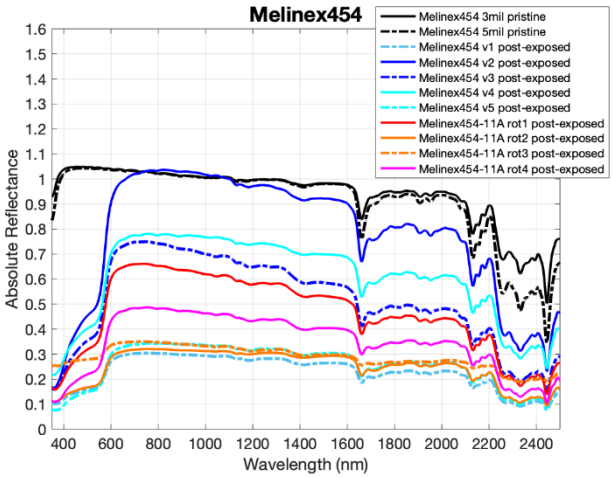

Fig. 16. Melinex 454 pre-exposure (pristine) in black and black dashed represent two different thicknesses. The initial post-exposure (teal, teal dash, blue, blue dash, and light blue) and the A series with multiple flat rotations in the instrument set-up (orange, orange dash, magenta, and red).

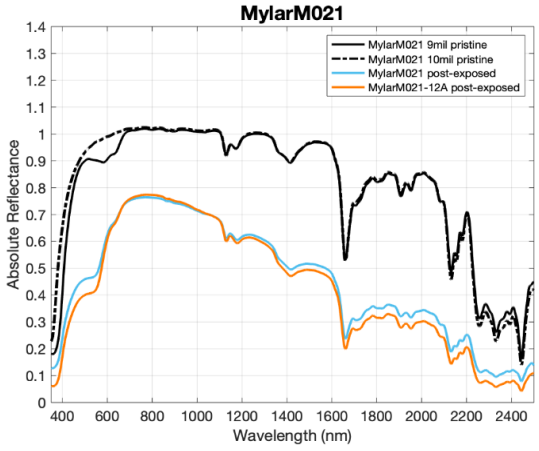

Fig. 17. Mylar M021 pre-exposure (pristine) in black compared to the initial post-exposure (blue) and the A series (orange).

The Mylar M021 sample comparisons show relatively similar features across all samples (pre- and post-exposure); however, the post-exposed spectra show an approximate 20% decrease in peak reflectance near 700 nm, as shown in Fig. 17. The pristine Mylar M021 shows a 450 nm to 400 nm bandgap due to white color, H2O (1400 nm and 1900 nm), C H or O-H bond triplet near 2100 nm, and C-H near 1650 nm and 2300 nm. The Mylar 9 mil sample (solid black line) showed an absorption feature near ~ 600 nm, which is also noted in white paints and previously measured Mylar samples but not present in the thicker 10 mil sample. The exposed Mylar has an approximate 20% decrease in peak reflectance near 700 nm, but overall, the exposed samples have consistent features with pristine. The 2450 nm feature present in both PET samples is consistent with C-O or O-H bonds in organic materials. Note that PET is constructed with C-H-O bonds (C12H14O4).

4.5. POSS

The CORIN XLS and Thermalbright® represent the POSS material class, where the CORIN XLS is transparent, and the Thermalbright N is optically white. The CORINXLS sample featured no organic features in the pristine sample, as shown in Fig. 18. The "squiggly line" in the pristine sample starting around 1000 nm is due to thin-film interference in the sample construction. The exposed CORIN XLS samples all indicate the presence of the experimental bias. In addition, the exposed CORINXLS samples also show a feature near 1600 nm and 2300 nm, most likely attributed to a carbon-hydrogen bond. At the present time, it is not clear if the presence of these organic features is from the exposed experimentation, the presence of the copper adhesive, or other chemical changes being investigated.

The Thermalbright sample comparisons show similar absorption features in the pristine and post-exposed data collects, with the exposed samples showing an approximate 10% decrease in reflectivity shown in Fig. 19. In addition, organic bonds near 2300 nm are much deeper in the exposed samples.

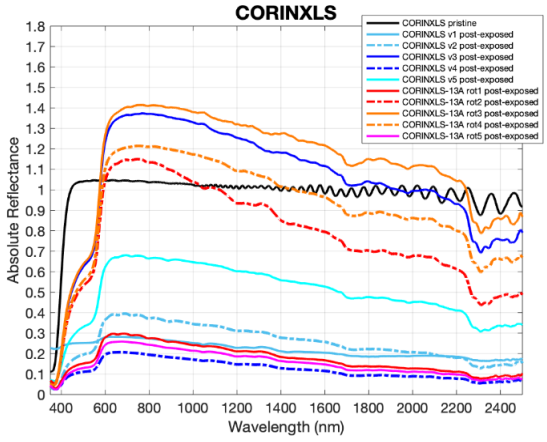

Fig. 18. CORIN XLS pre-exposure (pristine) in black compared to the initial post-exposure (teal, teal dash, blue, blue dash, and light blue) and the A series with multiple flat rotations in the instrument set-up (orange, orange dash, magenta, red, and red dash).

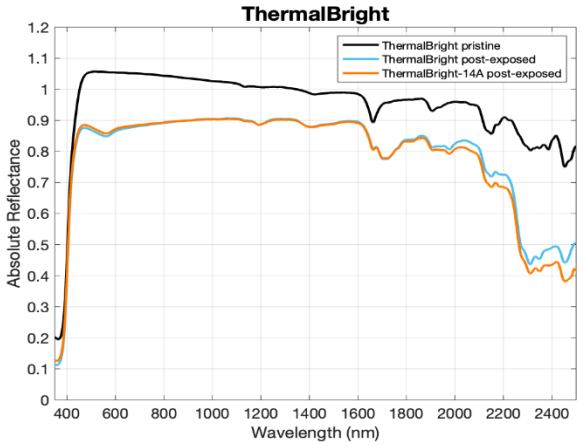

Fig. 19. Thermalbright pre-exposure (pristine) in black compared to the initial post-exposure (blue) and the A series (orange).

4.6. Alumina

The alumina material is presented with only post-electron exposure data, shown in Fig. 20. This material was not available to be measured in the OMC in pristine condition. Both spectral data collects are in close agreement to each other and exhibit similar spectral features. A minor, spectral signature is presented in the visible regime, similar to the signature noted previously between 400 nm to 550 nm, but with a steadily increasing slope. There are weak features at 1400 nm and 1900 nm, likely due to oxygen hydrogen bonds. The features at 1650 nm and 2300 nm are attributed to carbon-hydrogen bonds.

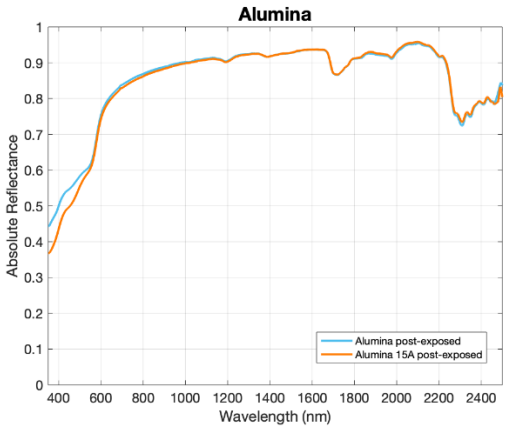

Fig. 20. Alumina comparisons between the initial post-exposure (blue) and the A series (orange). No pristine OMC measurements were available for comparison.

5. HCRF MEASUREMENTS

The following provides a summary and discussion on materials of interest from the subset presented in Table 3. Using commercial-off-the-shelf components, GTRI designed a goniometer system capable of characterizing the directional reflectance characteristics of materials within the principal plane of scattering. This goniometer was used to measure the HCRF of both the pristine and electron-exposed materials with fixed viewing angles (0°, 30°, 60°, -30°, and -60°) and variable illumination angles (0° - 70° degrees range). The goniometer relies upon a light source that provides collimated radiance onto the material sample under study. The light source optical assembly collimates illumination from a tungsten-halogen MR-16 bulb that simulates blackbody spectral irradiance over the range of 350 nm to 2500 nm. Radiance measurements throughout the measurement procedures are collected by an ASD FieldSpec 4, which contains three detectors spanning the same spectral range of 350 nm to 2500 nm.

The measurement procedure consists of two separate phases: an incident spectral irradiance characterization phase and a reflected spectral radiance measurement phase. The measurements resulting from these two phases are joined via a post-processing procedure to generate an HCRF measurement that allows for the finite angular extent of both the light source and sensor fore-optic. The derivation of the post-processing and the detailed outline of the goniometer system are fully outlined in a previous study [3].

5.1. PMDA

5.1.1. PMDA – Visibly Copper/Orange

Most PMDA materials see significant reductions in specularity as a result of aging via electron-bombardment. This can be observed in Fig. 21, in which pristine Kapton HN gives off a strong glint in the principal plane-viewing direction of $\theta_v = +30°$ due to light from an incident direction of $\theta_i = -30°$. The magnitude of this glint is reduced by a factor of ~3 across nearly all wavelengths after aging. The magnitude of the backscattered HCRF is also enhanced as a result of electron-bombardment aging, as can be seen in Fig. 22. The strength of the back-scattering HCRF appears to increase with the obliqueness of the illumination angle.

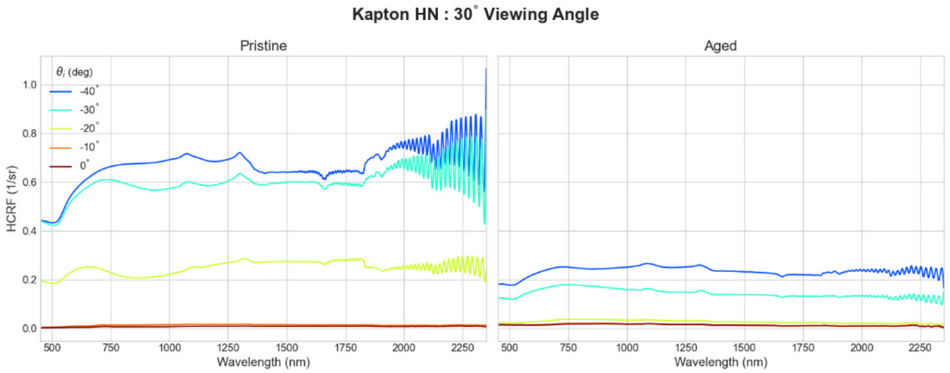

Fig. 21. Kapton HN HCRF measurements in the forward scattering viewing direction of $\theta_v = +30°$ for a variety of illumination directions θ_i.

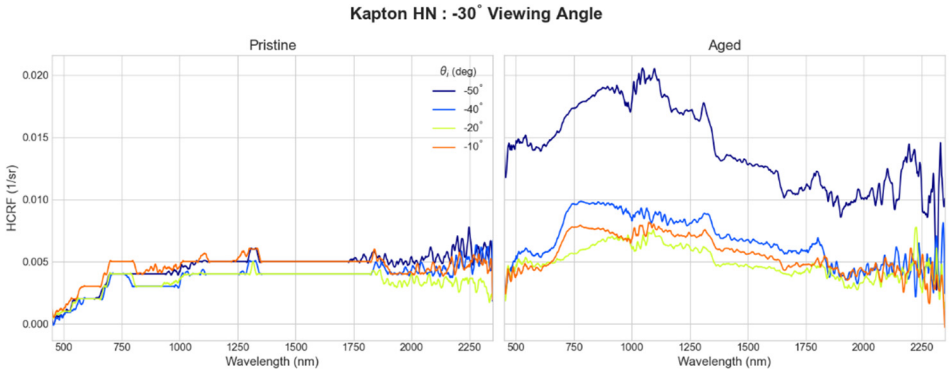

Fig. 22 Kapton HN HCRF measurements in the back-scattering viewing direction of $\theta_v = -30°$ for a variety of illumination directions θ_i in the principal plane.

5.1.2. PMDA – Visibly Black

The visibly black PMDA materials exhibited interesting spectral responses to the electron bombardment. As an example, the pristine Kapton XC material showed increasing specular scattering magnitude with wavelength ($\theta_i = -30°$ in left of Fig. 23). After aging, the specular scattering response was similar in magnitude over the spectral range of 450 nm to 1350 nm but dampened over the spectral range of 1400 nm to 2300 nm ($\theta_i = -30°$ in the right-hand side of Fig. 23). Furthermore, we can see that non-specular scattering directions were minimally affected by the aging experiments. We also observed that the Kapton XC showed increasing back-scatter HCRF magnitude after the aging experiments, as can be seen in Fig. 24.

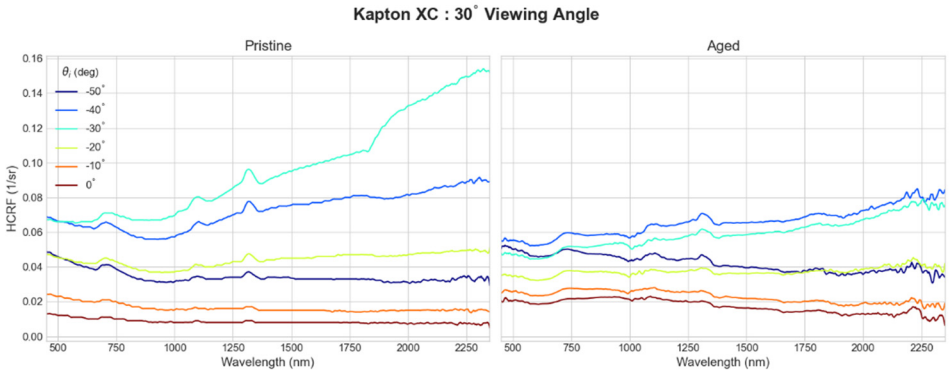

Fig. 23. Kapton XC HCRF measurements in the forward scattering viewing direction of $\theta_v = +30°$ for a variety of illumination directions θ_i.

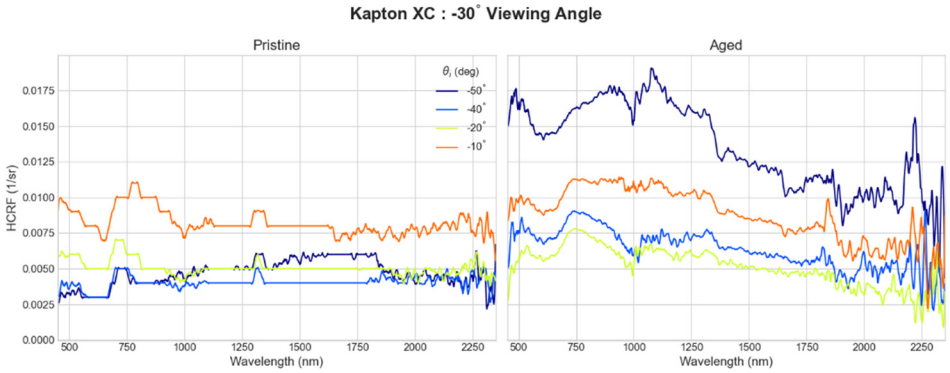

Fig. 24. Kapton XC HCRF measurements in the back-scattering viewing direction of $\theta_v = -30°$ for a variety of illumination directions θ_i in the principal plane.

5.2. CFRP

The CFRP material exhibited interesting spectral changes as a result of electron-bombardment for forward-scattering viewing directions in Fig. 25. In a pristine state, the material had an increasing slope of HCRF as a function of wavelength over the range of 1000 nm to 2300 nm. After aging, the material had a negative slope across all illumination angle directions considered in this study, as is shown in the right-hand side of Fig. 25.

Additionally, we can see that CFRP generally had a decreased HCRF magnitude across all wavelengths in the back-scattering direction. In Fig. 26, we see that illumination angles that are near the back-scattering lobe for the considered viewing direction of $\theta_v = -30°$ ($i.e. \theta_i = -20°$ and $-40°$) show a reduction in HCRF across all wavelengths.

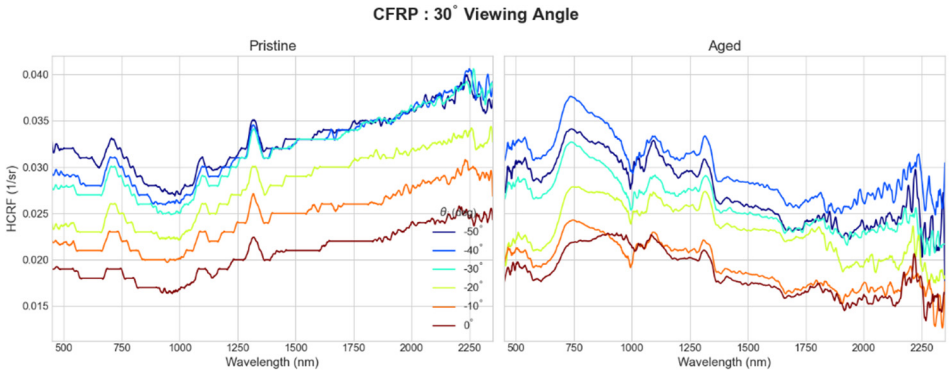

Fig. 25. CFRP HCRF measurements in the forward scattering viewing direction of $\theta_v = +30°$ for a variety of illumination directions θ_i.

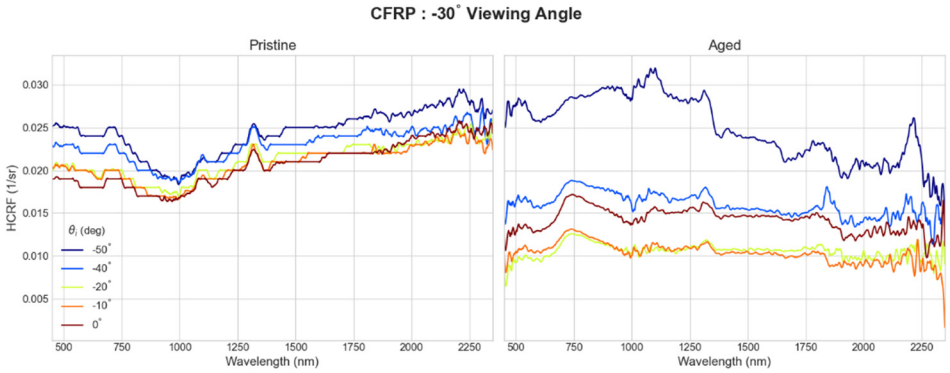

Fig. 26. CFRP HCRF measurements in the back-scattering viewing direction of $\theta_v = -30°$ for a variety of illumination directions θ_i in the principal plane.

5.3. LCP

Zenite LCP showed a reduction in HCRF magnitude across the entire spectrum of measured wavelengths in both the forward-scattering and back-scattering directions. Fig. 27 and Fig. 28 show that the general trend of decreasing HCRF magnitude with wavelength holds for both the aged and pristine samples over the spectral range of 500 nm to 2300 nm. Furthermore, we observed that the depth of the organic absorption features appears to shrink after the electron bombardment experiments.

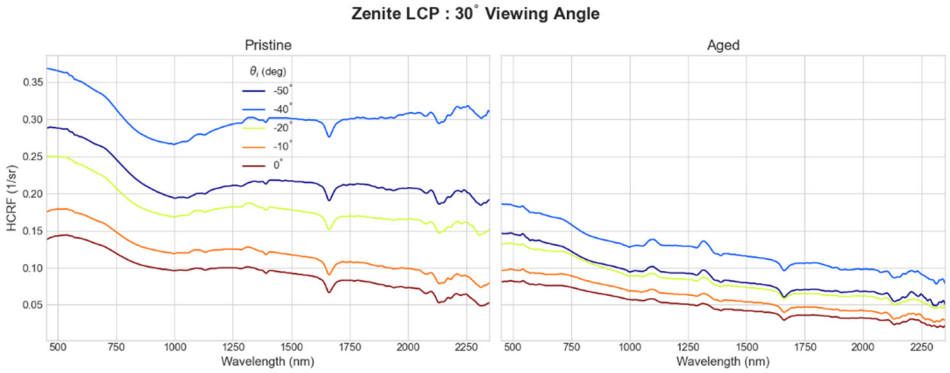

Fig. 27. LCP HCRF measurements in the forward scattering viewing direction of $\theta_v = +30°$ for a variety of illumination directions θ_i.

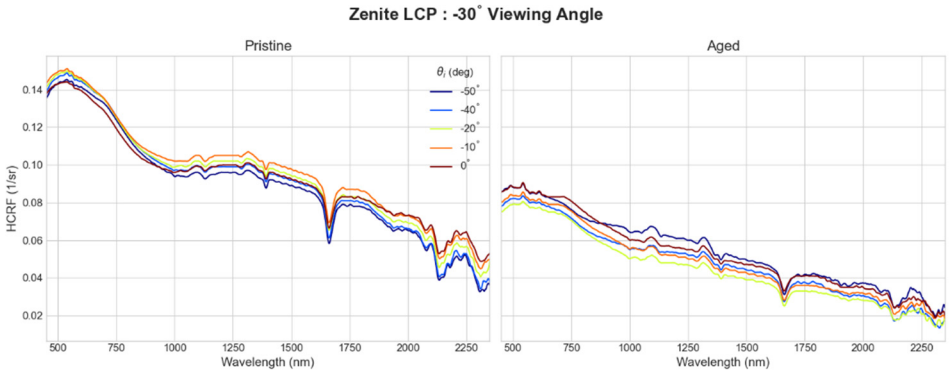

Fig. 28. LCP HCRF measurements in the back-scattering viewing direction of $\theta_v = -30°$ for a variety of illumination directions θ_i in the principal plane.

5.4. PET- Mylar M021

The 5 mil-thick Mylar M021 exhibited a large reduction in specular scattering magnitude as a result of electron-bombardment, as can be seen in Fig. 29. Interestingly, the off-specular scattering directions appear to be minimally affected by the electron bombardment aging. This can be seen by the spectra for pristine and aged measurements at illumination angles of $\theta_i = 0°$, -10°, and -50° in Fig. 29. The magnitude of back-scattered HCRF is similarly unaffected by the electron bombardment process. In Fig. 30, we show that the backscattering HCRF measurements for the pristine and aged Mylar materials are very similar in trend and magnitude across all considered wavelengths.

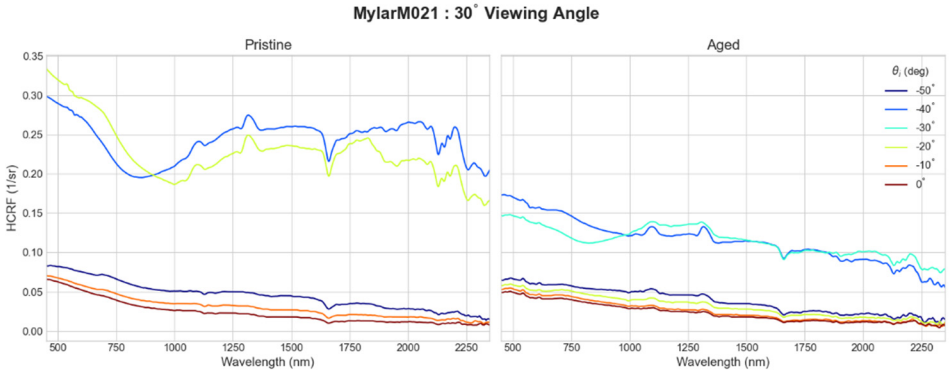

Fig. 29. Mylar ® M021 HCRF measurements in the forward scattering viewing direction of $\theta_v = +30°$ for a variety of illumination directions θ_i.

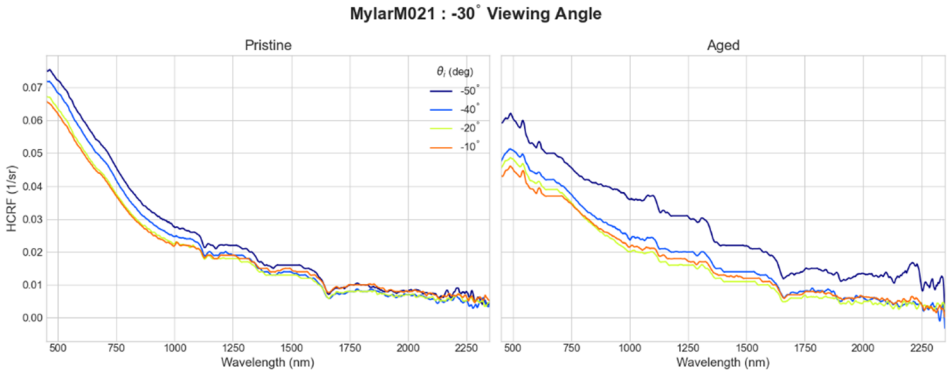

Fig. 30. Mylar ® M021 HCRF measurements in the back-scattering viewing direction of $\theta_v = -30°$ for a variety of illumination directions θ_i in the principal plane.

5.5. POSS - Thermalbright

The aging experiments that were carried out on Thermalbright resulted in a forward-scattering specular lobe that was significantly reduced in its angular spread. When measuring the pristine sample, we observed that the forward-scattering lobe was approximately 20° in angular extent based on the strong responses to illumination angles of θ_i= 20° and -40° in the left-hand side of Fig. 31. After electron-bombardment, we see that the HCRF strength in the mirror-like direction of the principal plane (i.e., θ_i= -30°) was similar in magnitude to that of the pristine sample. However, the HCRF magnitude due to illumination directions of θ_i= -20° and -40° was significantly reduced. Furthermore, we observed an interesting spectral trend in the aged experiments over the range of 1700 nm to 2300 nm in which the HCRF magnitude increased with wavelength.

For the back-scattering measurements in Fig. 32, we observed that there was a significant reduction in HCRF strength over the visible to near-infrared bandpass of 450 nm to 750 nm as a result of electron bombardment. However, the HCRF magnitude over the spectral range of 1000 nm to 2300 nm was minimally affected by the electron bombardment experiments.

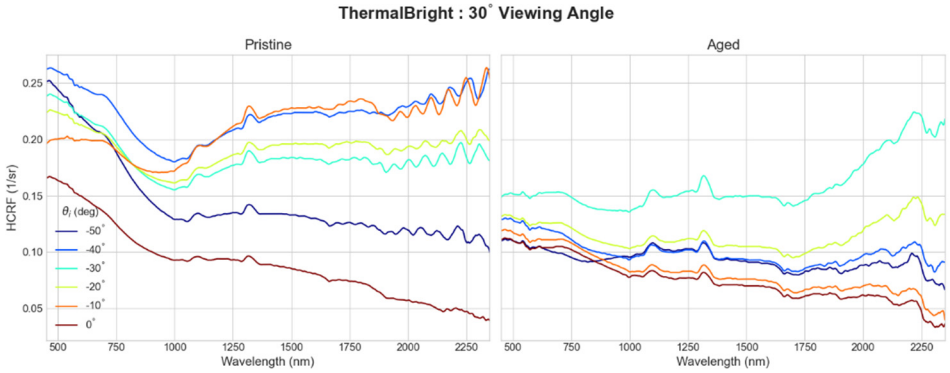

Fig. 31. Thermalbright HCRF measurements in the forward-scattering viewing direction of $\theta_v = +30°$ for a variety of illumination directions θ_i.

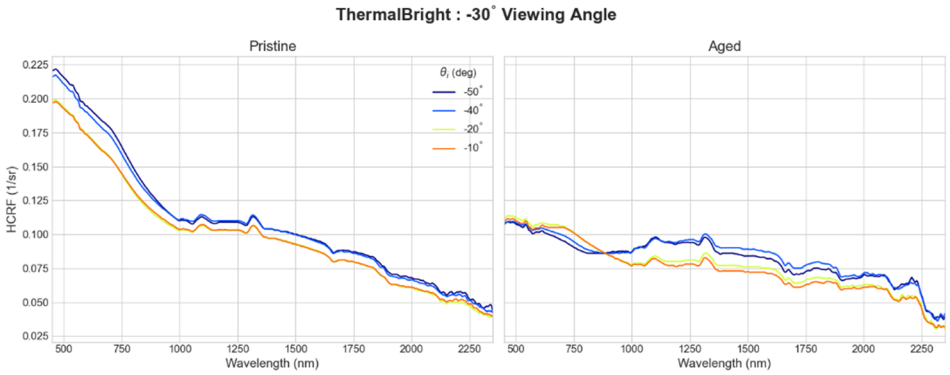

Fig. 32. Thermalbright HCRF measurements in the back-scattering viewing direction of $\theta_v = -30°$ for a variety of illumination directions θ_i in the principal plane.

6. SUMMARY

An overview of optical characterization on 15 samples to be flown on an upcoming MISSE-FF mission was presented. The data collected provides the reflectance spectra data and HCRF measurement data on samples in a pristine state and post-electron bombardment. A brief summary on the characterized materials is presented below.

- The PMDA materials (seven total - copper, white, and black), overall exhibited a decrease in reflectivity, but two of the copper Kapton samples (TF and HN) and white Kapton sample (CS) showed an increase in reflectivity. In addition, those same samples showed variability with rotation in the illumination set-up.
- The CFRP sample either increased in reflectivity or stayed relatively constant/with minor decrease, a function of the sample rotation after electron bombardment.

- The GFRP & LCP materials both showed a decrease in reflectivity over the entire spectrum after electron bombardment.
- The PET overall decreased in reflectivity after exposure, but the Melinex showed variations in reflectivity with sample rotations.
- The POSS materials, which were the thinnest of all samples evaluated, showed both an increase and a decrease in reflectivity with the CORIN XLS after exposure as a result of rotating the sample, but the Thermalbright showed an overall decrease.

Overall, the electron bombardment does affect the reflectance of these samples and a small subset appear to vary based on the illumination set-up. The forward plan includes finalizing AO exposure characterization and completing conductivity measurements at AFRL post-AO. The samples were successfully launched aboard Space-X CRS-25, in July 2022. The team looks forward to receiving the first data-package from the *in-situ* measurements.

7. DISCLAIMERS

Trade names and trademarks are used in this report for identification only. Their usage does not constitute an official endorsement, either expressed or implied, by the National Aeronautics and Space Administration.

The views expressed are those of the author and do not necessarily reflect the official policy or position of the Department of the Air Force, the Department of Defense, or the U.S. government.

The appearance of external hyperlinks does not constitute endorsement by the United States Department of Defense (DoD) of the linked websites, or the information, products, or services contained therein. The DoD does not exercise any editorial, security, or other control over the information you may find at these locations.

8. REFERENCES

[1] de Groh, K. and Banks, B. "MISSE-Flight Facility Polymers and Composites Experiment 1-4 (PCE 1-4)," NASA TM-20205008863, 2021. https://ntrs.nasa.gov/citations/20205008863

[2] https://www1.grc.nasa.gov/space/iss-research/misse/#misseflight-facility-misseff-missions

[3] Badura, G., Plis, E., and Valenta, C. Extending Laboratory BRDF Measurements towards Radiometric Modeling of Resident Space Object Spectral Signature Mixing, *Advanced Maui Optical and Space Surveillance Technologies Conference (AMOS)*, 2021.